Comparison of elastic properties of open-cell metallic biomaterials with different unit cell types

Hedayati, Reza; Sadighi, Mojtaba; Mohammadi-Aghdam, M; Hosseini-Toudeshky, H

DOI
10.1002/jbm.b.33854

Publication date
2018

Document Version
Final published version

Published in
Journal of Biomedical Materials Research. Part B: Applied Biomaterials

Citation (APA)
Hedayati, R., Sadighi, M., Mohammadi-Aghdam, M., & Hosseini-Toudeshky, H. (2018). Comparison of elastic properties of open-cell metallic biomaterials with different unit cell types. *Journal of Biomedical Materials Research. Part B: Applied Biomaterials*, *106*(1), 386-398. https://doi.org/10.1002/jbm.b.33854

Comparison of elastic properties of open-cell metallic biomaterials with different unit cell types

Reza Hedayati[a,b]*, Mojtaba Sadighi[a], Mohammad Mohammadi-Aghdam[a], Hossein Hosseini-Toudeshky[c]

[a]*Mechanical Engineering Department, Amirkabir University of Technology, Hafez Ave, Tehran, Iran,*

[b]*Department of Biomechanical Engineering, Faculty of Mechanical, Maritime, and Materials Engineering, Delft University of Technology (TU Delft), Mekelweg 2, 2628 CD, Delft, The Netherlands*

[c]*Aerospace Engineering Department, Amirkabir University of Technology, Hafez Ave, Tehran, Iran,*

*Corresponding author, Email: r.hedayati@tudelft.nl, rezahedayati@gmail.com

Abstract

Additive manufacturing techniques have made it possible to create open-cell porous structures with arbitrary micro-geometrical characteristics. Since a wide range of micro-geometrical features is available for making an implant, having a comprehensive knowledge of the mechanical response of cellular structures is very useful. In this study, finite element simulations have been carried out to investigate the effect of structure unit cell type (cube, rhombic dodecahedron, Kelvin, Weaire-Phelan, and diamond), cross-section type (circular, square, and triangular), strut length, and relative density on the Young's modulus, shear modulus, yield stress, shear yield stress, and Poisson's ratio of open-cell tessellated cellular structures. It was desired to see whether or not and to what extent each of the above-mentioned parameters affect the mechanical properties of a porous structure. It was seen that the strut cross-section type does not have a considerable effect on the structure Young's modulus while its effect on the structure yield stress is significant. The strut length was not effective on the mechanical properties if the relative density was kept constant. It was also observed that the structure unit cell type and

relative density have a considerable effect on the elastic properties. The highest and the lowest stiffness and strength belonged to the cube and diamond unit cell types, respectively. The rhombic dodecahedron structure with circular cross-section had a high yielding strength (second among all the cases) while its Young's modulus was relatively low. Therefore, it is the best choice for applications with low stiffness requirements, such as biomedical implants.

Keywords: Additive manufacturing; Open-cell foams; Porous biomaterials; Rhombic dodecahedron; Weaire-Phelan; Kelvin

Nomenclature

A	Cross-section area
b	Cross-section side
E_i	Porous structure Young's modulus in direction i
E_s	Solid material Young's modulus
G_{ij}	Shear modulus tensor
G_s	Solid material shear modulus
I	Area moment of inertia
r	Cross-section radius
K	Permeability
l	Strut length
l_f	Fluid flow course length
L_i	Unit-cell size in direction i
P	Pressure
Q	Permeate flux across the structure
γ_{ij}	Shear strain tensor
ε_i	Strain in direction i
ε_{ij}	Strain tensor
μ	Relative density
μ_f	Fluid dynamic viscosity
ρ	Porous structure density

ρ_s	Solid material density
σ	Applied external stress
σ_i	Applied stress in direction i
σ_{max}	Maximum stress in the struts
σ_y	Porous structure yield stress
σ_{y_s}	Bulk material yield stress
τ_{ij}	Shear stress tensor
ν_s	Solid material Poisson's ratio

1. Introduction

Metallic implants fabricated from materials such as titanium, tantalum, chrome, cobalt and stainless steel have been in routine clinical use for several years [1]. In more than 70% of cases, aseptic loosening is the cause for implant failure, often occurring relatively late after implantation [2, 3]. Important causes of aseptic loosening are micro-motions and stress shielding [2]. Micro-motions occur when the implant is free to slide in the medullary canal. It can be a result of too little bone ingrowth or mal-positioning of the implant [2, 4]. Stress shielding refers to the reduction in bone density (osteopenia) as a result of removal of normal stress from the bone by an implant [5, 6].

Today, metallic open-cell porous implants are replacing traditional solid implants because they significantly decrease the problems associated with solid implants, i.e. micro-motions and stress shielding. Since the ample spaces present inside the open-cell porous biomaterials allow for the transport of body fluids and therefore the ingrowth of new bone tissues, the implant attaches well to its surrounding natural bones reducing the relative micro-motions between the implant and the bone [7, 8]. The strength and the Young's modulus of the cellular materials can also be adjusted through the adjustment of the porosity to match the strength and stiffness of the natural bone [9].

Metal foams manufactured using traditional techniques usually have a morphology very similar to the one suggested by Weaire and Phelan [10] which is a complex 3D structure representing an idealized foam of equal-sized bubbles. Therefore, in the early years of development of porous biomaterials, the manufactured porous biomaterials had the Weaire-Phelan unit cell type [11]. The Weaire-Phelan unit cell type is not necessarily the most efficient unit cell type for biomedical applications. The mechanical properties and permeability of cellular structures heavily depend on their micro-geometrical specifications such as unit cell type, relative density, and pore size [12].

The advent of beam and powder-based layered manufacturing methods, such as selective laser melting (SLM) and selective electron beam melting (SEBM), made it possible to have precise control on the micro-architecture of cellular structures. Manufacturing of porous structures having arbitrary unit cell shape is the first and the most important result of this possibility. Using the additive manufacturing techniques, it is also possible to combine solid material with porous materials and also to combine porous materials with different micro-geometries in a single part [13].

Since the experimental verifications are time-consuming, expensive, and difficult to be performed, numerical simulations can provide significant help in designing open-cell biomaterials. A limited class of three-dimensional unit cell types can be packed together to create a tessellated cellular structure. Several studies have been carried out on selecting the appropriate unit cell types to manufacture biomimetic scaffolds aimed for bone tissue engineering [14, 15]. Cube [1, 16, 17], rhombic dodecahedron [2, 16, 18, 19], tetrakaidecahedrons [20-22], Weaire-Phelan [23, 24], and diamond [12, 16] are the most popular unit cell types which have been investigated mechanically before. Other micro-lattice structures such as body-centred cubic

structure (BCC) [25], body-centered cubic with vertical pillars (BCC-Z) [25], rhombicuboctahedron [26], truncated cube [27], facet-centered cubic with vertical pillars (FCC-Z) [28, 29], and truncated cuboctahedron [30] have also been investigated by different researchers. Although the mechanical response of each of the above-mentioned unit cell types at different relative densities have been presented singly in different studies, explicit comparisons of mechanical properties between different unit cell types is still vacant in the literature. Effect of cross-section type on the mechanical response of different unit cell types is also an important topic which has not been largely addressed previously.

Providing detailed comparison between the elastic properties of porous structures in terms of their unit cell type and cross-section type can be useful for applications in which low/high stiffness in axial/shear loadings is required. In this study, finite element (FE) simulations are implemented to investigate the effect of structure unit cell type, cross-section type, strut length, and relative density on the Young's modulus, shear modulus, yield stress, shear yield stress, and Poisson's ratio of open-cell tessellated cellular structures in a search to find the appropriate configuration for applications with low or high stiffness requirements. Five different unit cell types, namely cube, rhombic dodecahedron, Kelvin, Weaire-Phelan, and diamond with three different cross-section geometries (circle, square, and triangle) are considered. The mechanical properties of each case is obtained in relative densities ranging between μ=0 and μ=50%.

2. Materials and methods

Relative density, μ, is defined as the ratio of the density of the porous structure, ρ, to the density of the solid material, ρ_s, that the porous structure is made of. ANSYS APDL (ANSYS Parametric Design Language) was used to create automatic simulation loops in which relative density was varied from $\mu = 0$ to $\mu = 50\%$ for each unit cell type, and the resulted Young's

modulus and yield stress were measured. For each diagram, the mechanical properties were obtained for more than 40 relative densities. In each relative density, three different cross-section areas, i.e. $A = 15393\ \mu m^2$, $A = 37325.3\ \mu m^2$, and $A = 49087.4\ \mu m^2$ were taken into account and their results were compared. The cross-section dimensions (radius r for circular cross-sections and side b for square or triangular cross-sections) and the strut length were obtained for each unit cell type, relative density, cross-section type, and cross-section area using the formulas presented in [31]. Some examples of combinations of the strut cross-section size, strut length, and relative density is listed in the Table A1 in Appendix accompanying the paper.

The main mechanism of deformation in the microstructure of open-cell foams is bending of the struts making beam elements the natural choice for modeling open-cell structures. They are computationally inexpensive and can be used to compose models with many cells [32]. Therefore, all the struts of the open-cell foam model were mechanically represented by beams that were rigidly connected in vertices. The cell edges were descritized using standard Timoshenko beam element (element type 189 in ANSYS) that uses linear interpolation (two-node linear beam) and allows for transverse shear deformation. To check the accuracy of beam elements, as an example, the cubic structure was modeled using both beam elements and 3D volumetric elements. The results showed that the volumetric elements result in higher elastic moduli. However, the difference between the elastic moduli of the two types of elements was less than 4% even in relative densities as large as 30%.

In all the calculations, the cell edge material was assumed to be linear elastic. The material properties chosen for all the lattice structures were those of Ti-6Al-4V ELI alloy with Young's modulus of $E_s = 122.3\,GPa$, Poisson's ratio of $\nu_s = 0.342$, and yield stress of $\sigma_{y_s} = 980\ MPa$ [12].

The single unit cells inside the tessellated configurations of the five considered cellular structures are shown in Figure 1. In all the lattice structures, the bottom plane was fixed in the loading direction and the upper plane was displaced such that a homogenized compressive strain of 0.2% was generated in the tessellated structure. One of the nodes of the bottom plane was completely fixed in space to prevent the rigid body motion of the structure. The tessellated structures were free to move in the directions perpendicular to the loading direction, even in the lower and upper planes (Figure 2). To obtain the imposed stress on the structure (as a result of the applied external displacement), the resultant force of the lower plane in the Y direction was measured in each simulation. For each structure, the displacing procedure was repeated nine times to find the components of stress ($\sigma_{ij},\ i,j = 1,2,3$) caused by different strain types ($\varepsilon_{ij},\ i,j = 1,2,3$).

The Young's modulus of each tessellated structure in each direction i was calculated by dividing the resulted stress in the structure in that direction ($\sigma_i = F_i/A_i$) into the applied strain in that direction $\varepsilon_i = \delta_i/L_i$, where F_i, A_i, δ_i, and L_i are the resultant force, cross-sectional area, applied displacement, and length of the lattice structure in direction i, respectively. The shear modulus G_{ij} was calculated by dividing the resulted shear stress $\tau_{ij} = F_j/A_i$ into the corresponding applied shear strain $\gamma_{ij} = \delta_j/L_i$. Poisson's ratios were calculated by dividing the negative value of the resulted lateral strain by the imposed axial strain. In summary:

$$E_i = \frac{\sigma_i}{\varepsilon_i} \qquad i = 1,2,3 \qquad (1)$$

$$G_{ij} = \frac{\tau_{ij}}{\gamma_{ij}} \qquad i,j = 1,2,3 \qquad (2)$$

$$\nu_{ij} = \frac{\varepsilon_j}{\varepsilon_i} \qquad i,j = 1,2,3 \qquad (3)$$

For obtaining the yield stress of each lattice structure, first the maximum stress in the FE structure σ_{max} resulted from an arbitrary external stress imposed on the lattice structure σ was found. The imposed stress σ_y which causes the maximum stress in the struts of the lattice structure reach the bulk material yield stress σ_{y_s} can be found by a cross-multiply as $\sigma_y = \frac{\sigma}{\sigma_{max}} \sigma_{y_s}$. The yield stress of the bulk material was determined by offsetting the line overlying the linear part of the stress–strain curve to the right side for 0.2% of plastic strain and obtaining its intersection with the stress–strain curve. A similar procedure was done for obtaining the shear yield stress of bulk material.

For all the unit cell types but rhombic dodecahedron, the obtained elastic properties in different orientations, including the three Young's moduli, the six shear moduli, and the six Poisson's ratios were identical and therefore for each elastic property, only one value is reported. The rhombic dodecahedron structure has cubic transverse anisotropy and therefore two values are reported for each of its elastic properties.

Orientations of triangular cross-sections have a significant contribution on the obtained Young's modulus or yield stress of the lattice structure. In this study, in all the unit cell types, the orientation of the triangular cross-sections were chosen in such a way that the vertices became as symmetrical as possible. Considering symmetry when selecting the cross-section orientation has the advantage of decreasing the stress concentration in the vertices.

A structure size sensitivity analysis was performed to see in what size of structure, the Young's modulus of the lattice structure becomes very close to the Young's modulus of corresponding unlimited lattice structure. It was observed that the obtained Young's modulus values are less than 1% different for lattice structures with more than nine cells in each of the three main

directions of space (Figure 3). The number of elements per strut was changed from 1 to 10, and no change was observed in the obtained elastic modulus and maximum stress in the structure (using which the yield stress of the structure was found). Therefore, to reduce the computational time, two beam elements per strut was used for all the simulations.

Structures having the same relative density and unit cell type but with different strut lengths (i.e. pore size) or cross-sectional areas showed equal Young's modulus/yield stress. This is because if the relative density is kept constant and the strut length or cross-sectional area is changed, only the size of the representative volume element (RVE) is scaled, and the length ratio of different unit cell dimensions is not changed. This was proved for all the unit cell types and relative densities. The two parameters $\frac{r}{l}$ and μ are dependent variables. Therefore, if change in the value of Young's modulus or yield stress is needed, the cross-section type, unit cell type, and relative density (which is a sole function of $\frac{r}{l}$) must be changed. This is the consequence of a simple scaling of a linear-elastic solution under small deformations.

In this study, the values of Young's modulus, yield stress, shear modulus, shear yield stress, and Poisson's ratio will be compared between structures with different unit cell types at different relative densities. Effect of cross-section type on the yield stress and Young's modulus of these structures will also be compared. Finally, two comprehensive graphs comparing the Young's moduli and yield stresses of different unit cell and cross-section types will be presented using which implant manufacturers will be able to choose the right microstructural configuration depending on the required properties.

To validate the finite element models, the experimental elastic moduli and yield stresses values presented in other studies [1, 12, 13, 16, 17, 33, 34] for structures based on similar unit cells

were implemented. Similar to the numerical values, the experimental data were normalized with respect to the corresponding values of the bulk material. For normalizing the experimental data of porous structures based on rhombic dodecahedron, Weaire-Phelan, diamond, and cube, the mechanical properties of Ti-6Al-4V ($E_s = 113.8\,GPa$ and $\sigma_{ys} = 950\,MPa$) were used, while for normalizing the experimental data of porous structures based on Kelvin unit cell, the mechanical properties of HDDA polymer ($E_s = 530\,MPa$ and $\sigma_{ys} = 86\,MPa$) were implemented.

3. Results

3.1. Validation of the results

Both the elastic modulus vs. relative density and yield stress vs. relative density plots showed upward concave curves. In all the cases, the experimental values were higher than the numerical values. Generally, there was good numerical/experimental correlation in most the cases. The only case which showed large numerical/experimental discrepancy was the elastic modulus curve for structures based on cubic unit cell. Parthasarathy et al. [1] attributed this large experimental/numerical mismatch to "the melting of titanium alloy powder at high temperatures, and subsequent solidification by cooling causes an unevenness of the surface leading to cell surface curvatures and corrugation as seen in the SEM studies". In all the cases, the numerical/experimental correlation was better for smaller relative densities and it increased as the relative density increased.

3.2. Effect of unit cell type

To make comparison of the presented graphs to the graphs presented in other works easier, all the plots are presented in a normalized way, e.g. relative elastic modulus (the ratio of the elastic modulus of the porous structure to the elastic modulus of the bulk material), relative yield stress,

etc. The Young's moduli of different unit cell types are compared at different relative densities in Figure 5. It can be seen that the Young's modulus of rhombic dodecahedron structure in a direction is about twice of that in its other directions. The Young's modulus of the cubic structure was much higher than that of the other unit cell types (Figure 5). For example, at the relative density of 30%, the Young's modulus of the cubic structure was 3.63 times of that for the Weaire-Phelan structure, which was ranked second (after the cube). The Weaire-Phelan, Kelvin, and rhombic dodecahedron (in one of its main directions) structures had very close Young's moduli. The diamond structure had the lowest value of Young's modulus among all the unit cell types.

Yield stress (Figure 6) is another important factor in selecting the suitable unit cell type. As expected, in all the cases, the maximum stress occurred in the external surface of the critical struts. Like the Young's modulus, the lowest and the highest yield stress values belonged to the diamond and cubic structures, respectively. The rhombic dodecahedron was ranked second after the cube in terms of yield stress, and its yield stress in its two main directions were somewhat close (Figure 6).

In engineering load-bearing applications, higher values of yield stress is always favorable. However, this is not always true for the Young's modulus. In some applications such as medical implants, lower values of Young's modulus are more favorable. Since in some applications such as medical implants, high values of yield stress along with low values of stiffness are required, the parameter effective Young's modulus, which is the ratio of Young's modulus to yield stress of the material $\left(\frac{E}{\sigma_y}\right)$, was defined and investigated in this paper (Figure 7). Among all the cases, the two lowest effective Young's modulus values belonged to the two main directions of the

rhombic dodecahedron structure, therefore the rhombic dodecahedron structure shows the best performance for the applications in which low values of stiffness is required. The cubic structure had the highest stiffness/yield stress ratio and is therefore the least favorable choice for medical implants. The Weaire-Phelan structure (the morphology of traditional foams) also shows a weak performance and is the second less attractive choice for bone-replacing biomaterials (Figure 7).

In most applications, the foam must also have good stiffness and strength against shear forces. While the rhombic dodecahedron structure had the lowest effective Young's modulus (Figure 7), it possessed the highest shear modulus among all the unit cell types (Figure 8). Therefore, it can be a good candidate for cases in which high values of shear stiffness is required. It must be kept in mind that the rhombic dodecahedron does not show a high shear stiffness in its second direction, therefore its orientation with main loading directions must be considered while designing an implant. As of the axial case (Figure 5), the diamond structure had the lowest value of shear modulus (Figure 8). The rhombic dodecahedron and diamond unit cell types had the highest and the lowest shear yield stresses, respectively (Figure 9).

Figure 10 compares the Poisson's ratio values for different unit cell types. The cube structure showed a zero Poisson's ratio. It is because in the cube structure, none of the struts go under bending. The struts parallel to the loading direction simply shrink and the struts perpendicular to the loading direction do not deform. They just move translationally parallel to the loading direction. Since the struts in other unit cell types go under bending, their Poisson's ratio is not zero. The diamond and rhombic dodecahedron structures showed the highest Poisson's ratio in the relative densities smaller and larger than 36%, respectively. Weaire-Phelan structure always showed the lowest Poisson's ratio (Figure 10). In Weaire-Phelan and diamond structures,

increasing the relative density always decreased the Poisson's ratio. However, the rhombic dodecahedron and Kelvin structures showed concave upward Poisson's ratio curves (Figure 10).

3.3. Effect of cross-section geometry

In addition to unit cell type, the cross-section geometry type also affects the response of the porous structure. In this study, three different cross-section geometries namely circle (C), square (S), and triangle (T) were considered for comparison. The cross-section type had very minor effects on the Young's modulus value. The highest and the lowest Young's moduli of each unit cell type belonged to the triangular and circular cross-sections, respectively, (Figure 11).

Unlike the Young's modulus, the yield stress value was heavily affected by the cross-section type (Figure 12). Its effect was in such a way that among all the cases with different unit cell and cross-section types, the three cases with the highest yield stress values all had circular cross-section types, while the triangular cross-section type led to the lowest yield stress values (Figure 12). Therefore, it can be concluded that the circular cross-section type increases the resistance of the lattice structure against yielding greatly while not changing its Young's modulus considerably. The rhombic dodecahedron structure with circular cross-section type had a high yielding strength (second among all the cases, Figure 12) while its Young's modulus was somewhat low (Figure 11). Therefore, it is the best choice for applications with low stiffness requirements, such as biomedical implants. This is better depicted if the *effective* Young's modulus is plotted for all the cases in a single graph (Figure 13).

3.4. Effect of relative density

In all the figures plotted before, it was seen that increasing the relative density increases both the Young's modulus and yield stress. Increasing the relative density from 10% to 30% increased the

Young's moduli of the cube, diamond, Kelvin, rhombic dodecahedron, and Weaire-Phelan structures for 218%, 573%, 500%, 571%, and 468%, respectively (Figure 5). Increasing the relative density from 10% to 30% increased the yield stress of the cube, diamond, Kelvin, rhombic dodecahedron, and Weaire-Phelan structures for 218%, 407%, 304%, 340%, and 397% respectively (Figure 6). Therefore, increasing the relative density has the most and less increasing effect on the diamond and cube structures, respectively.

4. Discussions

Before the advent of additive manufacturing technologies, several manufacturing techniques, such as powder metallurgy, laser and plasma arc welding of powders, self-propagating high-temperature synthesis, pressing of metallic powders with filler and its subsequent removal, pressure casting of powder metals and alloys were used to construct open-cell foams [35]. The metal foams manufactured using the above-mentioned methods usually have random micro-structures and non-uniform distribution of micro-mechanical properties. Even at the same relative density, the macro-mechanical properties of porous structures made by different fabrication technologies can be very different. For example, Rubshtein et al. [35] reported that at the relative density of 40%, the Young's modulus of porous structures made by different fabrication technologies can differ for more than 2.5 times. The additive manufacturing techniques provide the user with uniform microarchitecture with arbitrary geometrical, and therefore mechanical, properties.

In this paper, five well-known unit cell types were numerically investigated and their mechanical properties were obtained and compared to each other. The presented unit cell types demonstrated wide ranges of Young's modulus and yield stress for both the axial and shear loads. Depending on the body part, the person's age and sex, and the direction and location of the natural bone

used for mechanical testing, the obtained mechanical properties for the bone can be very different. Using the elastic properties diagrams presented in this study, and depending on the required mechanical properties, a computer program can be used to create implants with variable relative densities, cross-section types, and even unit cell types at their different regions. Using CT images, the manufactured implants can have tailored mechanical properties that mimic the stiffness of each patient's bone to reduce stress shielding and therefore increase bone modeling [36].

The results of the mechanical properties of the five unit cell types presented in this paper are comprehensive since they include Poisson's ratio and Young's and shear modulus and yield stress for three different cross-section types. As mentioned above, all the cell types except rhombic dodecahedron show a cubic anisotropic behavior. In cubic anisotropic materials, the obtained Young's moduli for the three main directions (which are equal) are not true for diagonal directions. The same is true if the loading direction is diagonal and not parallel to the main directions of the unit cell. Compared to bulk materials, the dependency of shear modulus to the Young's modulus is much lower in porous structures. To predict the Young's modulus in directions rather than the main directions, the superposition principle can be used. The diagonal loads can be decomposed into components parallel and perpendicular to the unit cell main directions. The Young's modulus and Poisson's ratio of the structure in the diagonal directions can be obtained by obtaining the resulted displacement in the main directions due to different load components and then superimposing them.

Some parts of the results presented in this work have already been published by other researchers. The shear modulus, shear yield stress, and Poisson's ratio of the five unit cell types presented in this paper have not been studies before. Moreover, the explicit comparison of the

elastic properties of these structures has not been done before. Investigation of the effect of cross-section geometry and strut length on the elastic properties of the lattice structures is the other novelty of the current study.

Comparison of our numerical results with the numerical and analytical results provided in other works can be of interest. The mismatch between our results and the existing results is caused by the method of calculating the relative density. Reviewing the literature revealed that researchers [2, 12, 17-19, 37-40] usually simply multiply the strut length in their cross-section area to find the structure mass from which the relative density can be calculated. In our study, the material located in the vertices are not counted multiple times (known as multiple counting effect [31]). This leads to smaller relative densities at the same mechanical property. The effect of multiple counting of material mass in the vertices becomes more critical when the thickness of the struts are larger. This is why the mismatch between the results presented in this paper and the existing data is very small at smaller relative densities and increases by increasing the relative density. Since in different studies, the method of obtaining the relative density for numerical study is different, in the following, our numerical studies are compared to the corresponding numerical studies in different r/l ratios rather than in different relative densities. For the diamond, rhombic dodecahedron, and cubic structures, our numerical results are very close and always higher than the corresponding numerical results in [12, 16] (Figure 14). The FE models in [12, 16] have also considered the manufacturing irregularities created in the additively manufactured porous biomaterials. Therefore, they always have predicted lower Young's moduli.

The struts of two structures with the same unit cell type and relative density but with different cross-section geometries have the same cross-sectional areas. Due to identical cross-sectional area, the mechanical response of the struts with different cross-section types are similar in pure

tension/compression. However, they respond differently in bending because their area moment of inertia is unequal. Higher values of area moment of inertia decreases the deflection which makes the lattice structure have a larger Young's modulus. This explains the descending order of Young's modulus in the structures with triangular ($I = \frac{A^2}{18/\sqrt{3}} \approx 0.096\, A^2$), square ($I = \frac{A^2}{12} \approx 0.083\, A^2$), and circular ($I = \frac{A^2}{4\pi} \approx 0.08\, A^2$) cross-section types (Figure 11).

In this study, it was shown that pore size is not a determinative factor in the resulted mechanical properties. However, pore size can be effective on the ease at which liquid flows into a porous structure at a particular pressure gradient [41], or permeability. Permeability in low Reynold's numbers (laminar flows) is measured by Darcy's law $K = \mu_f l_f Q/\Delta P$, where μ_f is the fluid dynamic viscosity, Q is the permeate flux across the structure, l_f is the course length through which the flow passes, and ΔP is the pressure gradient. Higher permeability allows for better vascular invasion and nutrients supply required to sustain cell growth which then provides better osseointegration. Pore sizes used for biomedical implants usually are in the range of $75\ \mu m$ to $800\ \mu m$ [16, 41-43]. A study by Schek et al. [44] showed that at the same relative density (50%), bone regeneration is not affected by pore sizes between 300 and $800\ \mu m$ in PPF/b-TCP scaffolds after 4 weeks. A similar conclusion was made by Roosa et al. [45] who showed that for pore sizes between 350 and $800\ \mu m$, bone growth inside pores is depended on pore size at 4 weeks (the scaffold bone volume is almost twice for the scaffold with $800\ \mu m$ pore size with respect to scaffold with $350\ \mu m$ pore size) but not at 8 weeks. Although pore size might not be effective on the bone ingrowth in long time periods, higher bone ingrowth of the porous biomaterials with larger pore size in the initial weeks after implantation can lead to their better fixation and their

longer durability. The pore size might also have some effects on the fatigue response of a biomaterial (as shown in [13, 46]).

Designing a suitable biomedical implant consists of consideration of several factors (some of which are independent from the others) including material (which must be selected based on the desired bio-compatibility, corrosion-resistance, cost, etc.), pore size (which has to be selected based on the desirable permeability in short times after implantation), strut cross-section type (which influences yield stress), relative density (the value of which heavily affects both the elastic properties and permeability), and unit cell type. Among the above-mentioned factors, the dependent factors are the three steps of choosing the appropriate relative density (which affects both the mechanical properties and permeability), pore size (which affects the permeability), and unit cell type (which affects both the mechanical properties and permeability). The obtained results in this study provide a comprehensive library of elastic properties for five different unit cell types with three different cross-section types in a large range of relative densities. A similar work can be done on permeability. The two sets of results can be useful for an implant manufacturer to choose the most optimum geometrical parameters for a particular implant.

The results of study was based on porous structures with no defect. In practice, the additively manufactured porous structures have several imperfections such as rough strut surfaces, change in the length of the struts, etc. The direction of printing can also affect the mechanical response of the additively manufactured parts [47]. Processing parameters [48] such as laser power and exposure time can also be effective on the micro-pore size, the degree of roughness, the microstructural grain shaper and size, etc. A numerical design procedure should be composed of two main phases: in the first phase, the porous structure can have an ideal geometry. An optimization algorithm can determine the optimum distribution of unit cell type, relative density,

and strut geometry to give the desired results. In the second phase, the effect of other influencing factors such as processing parameters, printing direction, degree of roughness, etc. can be taken into account to make the numerical model capable of predicting the actual mechanical properties of additively manufactured porous structure.

5. Conclusions

In this work, FE simulations were carried out to investigate the effect of structure unit cell type, cross-section type, strut length, and relative density on the Young's modulus, shear modulus, yield stress, shear yield stress, and Poisson's ratio of open-cell tessellated cellular structures in a search to find the appropriate configuration for applications with low-stiffness or high-stiffness requirements. Based on the results obtained in this study, it can be concluded that:

- The cube and the diamond unit cell types respectively have the highest and the lowest Young's moduli among all the cases.
- Similarly, the cube and the diamond structures have the highest and the lowest *yield stress* values among all the unit cell types. The rhombic dodecahedron is ranked second after the cube in terms of yield stress.
- The rhombic dodecahedron and cubic structures have the highest shear modulus values. Therefore, they are good candidates for cases in which high values of shear stiffness is needed.
- For all the unit cell types, the triangular and the circular cross-sections lead to the highest and lowest Young's moduli, respectively, although the cross-section type has only very minor effects on the Young's modulus value.

- Unlike the Young's modulus, the *yield stress* value is heavily affected by the cross-section type. Its effect is in such a way that among all the configurations with different unit cell types and different cross-section types, the three configurations with the highest values of yield stress all had circular cross-sections. The triangular cross-section leads to the lowest yield strength values.
- The rhombic dodecahedron structure with circular cross-section type has a high yielding strength (second among all the cases) while its Young's modulus is somewhat low. Therefore, it is the best choice for applications with low stiffness requirements, such as biomedical implants.
- The cube structure shows very high Young's modulus and yield stress values, therefore it is a good candidate for applications with high stiffness requirements.

References

1. Parthasarathy, J., et al., *Mechanical evaluation of porous titanium (Ti6Al4V) structures with electron beam melting (EBM).* Journal of the mechanical behavior of biomedical materials, 2010. **3**(3): p. 249-259.
2. Borleffs, M., *Finite element modeling to predict bulk mechanical properties of 3D printed metal foams*. 2012, TU Delft, Delft University of Technology.
3. Sundfeldt, M., et al., *Aseptic loosening, not only a question of wear: a review of different theories.* Acta orthopaedica, 2006. **77**(2): p. 177-197.
4. Bougherara, H., et al., *Design of a biomimetic polymer□composite hip prosthesis.* Journal of Biomedical Materials Research Part A, 2007. **82**(1): p. 27-40.
5. Sing, S.L., et al., *Laser and electron□beam powder□bed additive manufacturing of metallic implants: A review on processes, materials and designs.* Journal of Orthopaedic Research, 2016. **34**(3): p. 369-385.
6. Sing, S.L., W.Y. Yeong, and F.E. Wiria, *Selective laser melting of titanium alloy with 50 wt% tantalum: Microstructure and mechanical properties.* Journal of Alloys and Compounds, 2016. **660**: p. 461-470.
7. Zardiackas, L.D., et al., *Structure, metallurgy, and mechanical properties of a porous tantalum foam.* Journal of biomedical materials research, 2001. **58**(2): p. 180-187.
8. Clemow, A., et al., *Interface mechanics of porous titanium implants.* Journal of Biomedical Materials Research, 1981. **15**(1): p. 73-82.
9. Wen, C., et al., *Processing of biocompatible porous Ti and Mg.* Scripta Materialia, 2001. **45**(10): p. 1147-1153.
10. Weaire, D. and R. Phelan, *A counter-example to Kelvin's conjecture on minimal surfaces.* Philosophical Magazine Letters, 1994. **69**(2): p. 107-110.

11. Gomez, S., et al., *Characterization and three-dimensional reconstruction of synthetic bone model foams.* Materials Science and Engineering: C, 2013. **33**(6): p. 3329-3335.
12. Ahmadi, S., et al., *Mechanical behavior of regular open-cell porous biomaterials made of diamond lattice unit cells.* Journal of the mechanical behavior of biomedical materials, 2014. **34**: p. 106-115.
13. Amin Yavari, S., et al., *Fatigue behavior of porous biomaterials manufactured using selective laser melting.* Materials Science and Engineering: C, 2013. **33**(8): p. 4849-4858.
14. Cheah, C., et al., *Development of a tissue engineering scaffold structure library for rapid prototyping. Part 1: investigation and classification.* The International Journal of Advanced Manufacturing Technology, 2003. **21**(4): p. 291-301.
15. Fantini, M., M. Curto, and F. De Crescenzio, *A method to design biomimetic scaffolds for bone tissue engineering based on Voronoi lattices.* Virtual and Physical Prototyping, 2016. **11**(2): p. 77-90.
16. Campoli, G., et al., *Mechanical properties of open-cell metallic biomaterials manufactured using additive manufacturing.* Materials & Design, 2013. **49**: p. 957-965.
17. Gibson, L.J. and M.F. Ashby, *Cellular solids: structure and properties*. 1997: Cambridge university press.
18. Shulmeister, V., et al., *A numerical study of large deformations of low-density elastomeric open-cell foams.* Mechanics of materials, 1998. **30**(2): p. 125-140.
19. Babaee, S., et al., *Mechanical properties of open-cell rhombic dodecahedron cellular structures.* Acta Materialia, 2012. **60**(6): p. 2873-2885.
20. Warren, W. and A. Kraynik, *Linear elastic behavior of a low-density Kelvin foam with open cells.* Journal of Applied Mechanics, 1997. **64**(4): p. 787-794.
21. Storm, J., et al., *Geometry Dependent Effective Elastic Properties of Open□Cell Foams Based on Kelvin Cell Models***.* Advanced Engineering Materials, 2013. **15**(12): p. 1292-1298.
22. Demiray, S., W. Becker, and J. Hohe, *Numerical determination of initial and subsequent yield surfaces of open-celled model foams.* International journal of solids and structures, 2007. **44**(7): p. 2093-2108.
23. Daxner, T., R.D. Bitsche, and H.J. Böhm, *Space-filling polyhedra as mechanical models for solidified dry foams.* Materials transactions, 2006. **47**(9): p. 2213-2218.
24. Buffel, B., et al., *Modelling open cell-foams based on the Weaire–Phelan unit cell with a minimal surface energy approach.* International Journal of Solids and Structures, 2014. **51**(19): p. 3461-3470.
25. Smith, M., Z. Guan, and W. Cantwell, *Finite element modelling of the compressive response of lattice structures manufactured using the selective laser melting technique.* International Journal of Mechanical Sciences, 2013. **67**: p. 28-41.
26. Hedayati, R., et al., *Mechanics of additively manufactured porous biomaterials based on the rhombicuboctahedron unit cell.* Journal of the Mechanical Behavior of Biomedical Materials, 2016. **53**: p. 272–294.
27. Hedayati, R., et al., *Mechanical properties of regular porous biomaterials made from truncated cube repeating unit cells: analytical solutions and computational models.* Materials Science and Engineering: C, 2016. **60**: p. 163-183.
28. Labeas, G. and M. Sunaric, *Investigation on the static response and failure process of metallic open lattice cellular structures.* Strain, 2010. **46**(2): p. 195-204.
29. Niendorf, T., F. Brenne, and M. Schaper, *Lattice Structures Manufactured by SLM: On the Effect of Geometrical Dimensions on Microstructure Evolution During Processing.* Metallurgical and Materials Transactions B, 2014. **45**(4): p. 1181-1185.
30. Hedayati, R., et al., *Mechanical behavior of additively manufactured porous biomaterials made from truncated cuboctahedron unit cells.* International Journal of Mechanical Sciences, 2016. **106**: p. 19-38.

31. Hedayati, R., et al., *Effect of mass multiple counting on the elastic properties of open-cell regular porous biomaterials.* Materials & Design, 2016. **89**: p. 9–20.
32. Daxner, T., *Finite element modeling of cellular materials*, in *Cellular and Porous Materials in Structures and Processes*. 2010, Springer. p. 47-106.
33. Zheng, X., et al., *Ultralight, ultrastiff mechanical metamaterials.* Science, 2014. **344**(6190): p. 1373-1377.
34. Heinl, P., C. Körner, and R.F. Singer, *Selective electron beam melting of cellular titanium: mechanical properties.* Advanced Engineering Materials, 2008. **10**(9): p. 882-888.
35. Rubshtein, A., et al., *Porous material based on spongy titanium granules: Structure, mechanical properties, and osseointegration.* Materials Science and Engineering: C, 2014. **35**: p. 363-369.
36. Harrysson, O.L., et al., *Direct metal fabrication of titanium implants with tailored materials and mechanical properties using electron beam melting technology*. Materials Science and Engineering: C, 2008. **28**(3): p. 366-373.
37. Ushijima, K., et al., *An investigation into the compressive properties of stainless steel micro-lattice structures.* Journal of Sandwich Structures and Materials, 2010.
38. Gent, A. and A. Thomas, *Mechanics of foamed elastic materials.* Rubber Chemistry and Technology, 1963. **36**(3): p. 597-610.
39. Ptochos, E. and G. Labeas, *Elastic modulus and Poisson's ratio determination of micro-lattice cellular structures by analytical, numerical and homogenisation methods.* Journal of Sandwich Structures and Materials, 2012: p. 1099636212444285.
40. Ptochos, E. and G. Labeas, *Shear Modulus Determination of Cuboid Metallic Open□Lattice Cellular Structures by Analytical, Numerical and Homogenisation Methods.* Strain, 2012. **48**(5): p. 415-429.
41. Zhang, Z., et al., *Hierarchical tailoring of strut architecture to control permeability of additive manufactured titanium implants.* Materials Science and Engineering: C, 2013. **33**(7): p. 4055-4062.
42. Despois, J.-F. and A. Mortensen, *Permeability of open-pore microcellular materials.* Acta Materialia, 2005. **53**(5): p. 1381-1388.
43. Shimko, D.A., et al., *Effect of porosity on the fluid flow characteristics and mechanical properties of tantalum scaffolds.* Journal of Biomedical Materials Research Part B: Applied Biomaterials, 2005. **73**(2): p. 315-324.
44. Schek, R.M., et al., *Combined use of designed scaffolds and adenoviral gene therapy for skeletal tissue engineering.* Biomaterials, 2006. **27**(7): p. 1160-1166.
45. Roosa, S.M.M., et al., *The pore size of polycaprolactone scaffolds has limited influence on bone regeneration in an in vivo model.* Journal of Biomedical Materials Research Part A, 2010. **92**(1): p. 359-368.
46. Hedayati, R., et al., *Computational prediction of the fatigue behavior of additively manufactured porous metallic biomaterials* International journal of fatigue, 2016. **84**: p. 67–79.
47. Kok, Y., et al., *Fabrication and microstructural characterisation of additive manufactured Ti-6Al-4V parts by electron beam melting: This paper reports that the microstructure and micro-hardness of an EMB part is thickness dependent.* Virtual and Physical Prototyping, 2015. **10**(1): p. 13-21.
48. Sing, S., et al., *Characterization of titanium lattice structures fabricated by selective laser melting using an adapted compressive test method.* Experimental Mechanics, 2016. **56**(5): p. 735-748.

Figure captions

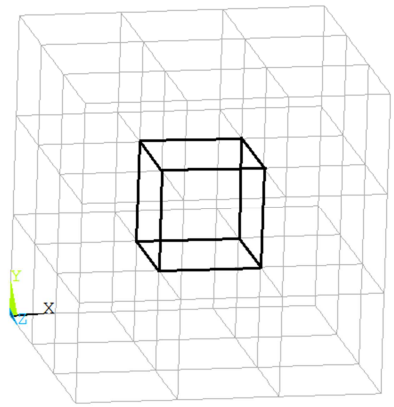

Cube

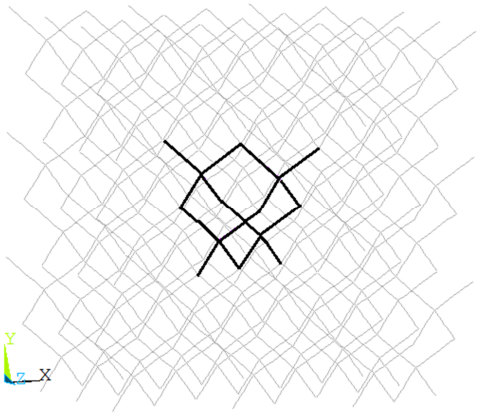

Diamond

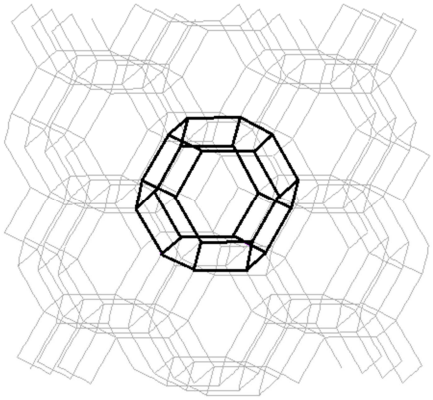

Kelvin

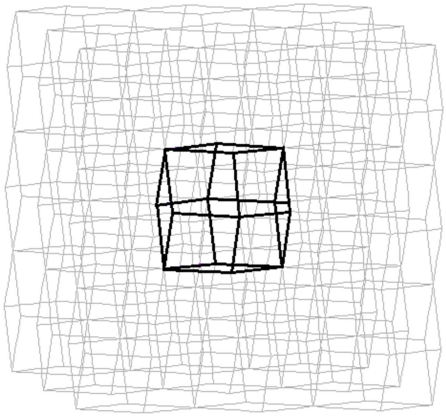

Rhombic dodecahedron

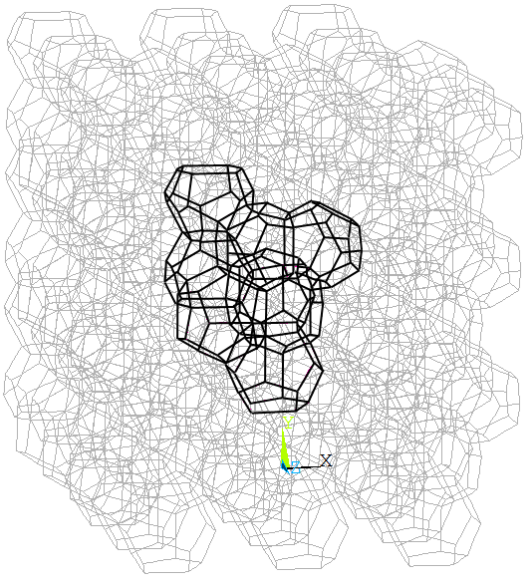

Weaire-Phelan

Figure 1- Graphical view of different unit cells inside a 3×3 lattice structure

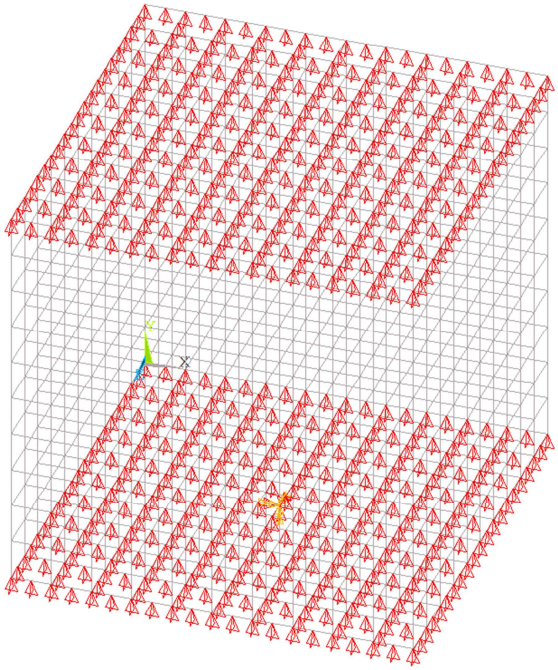

(a)

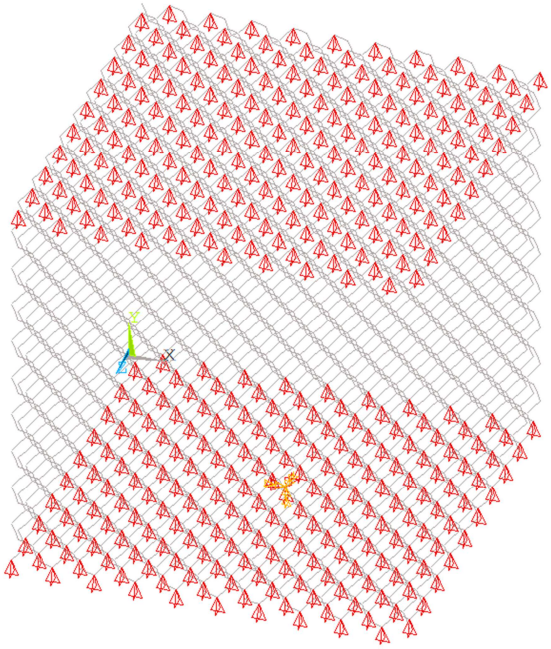

(b)

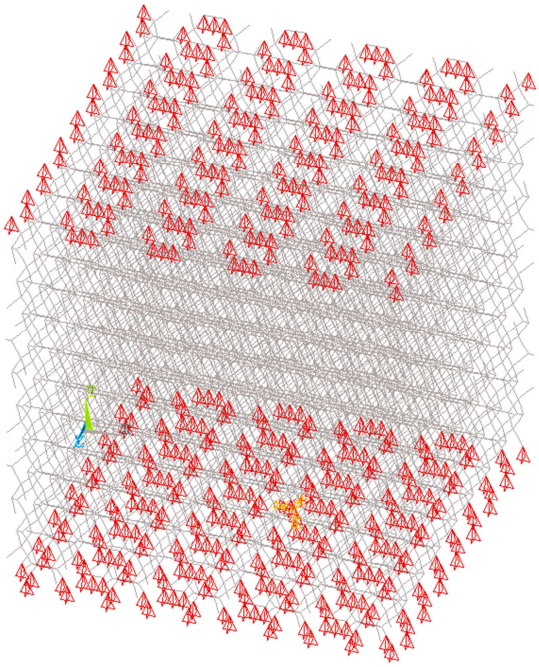

(c)

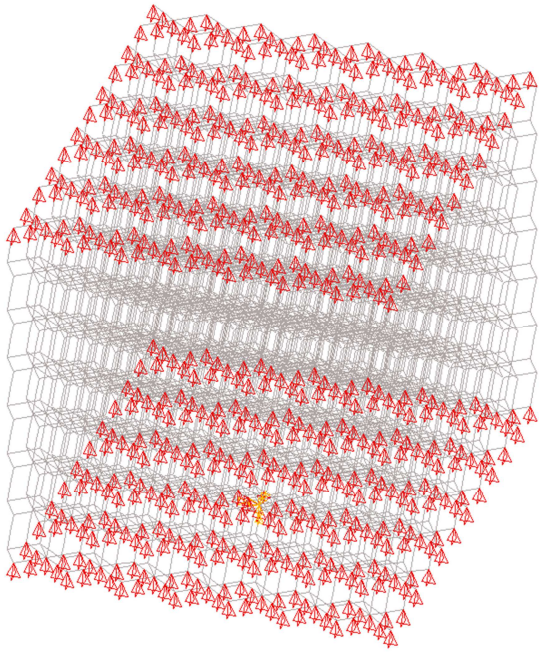

(d)

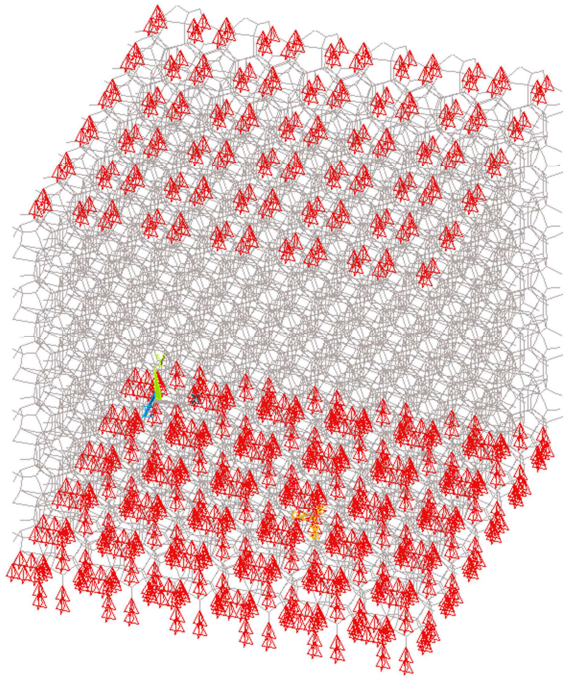

(e)

Figure 2- Boundary conditions and 3D views of lattice structures with the five unit cell types: (a) cube, (b) diamond, (c) Kelvin, (d) rhombic dodecahedron, and (e) Weaire-Phelan

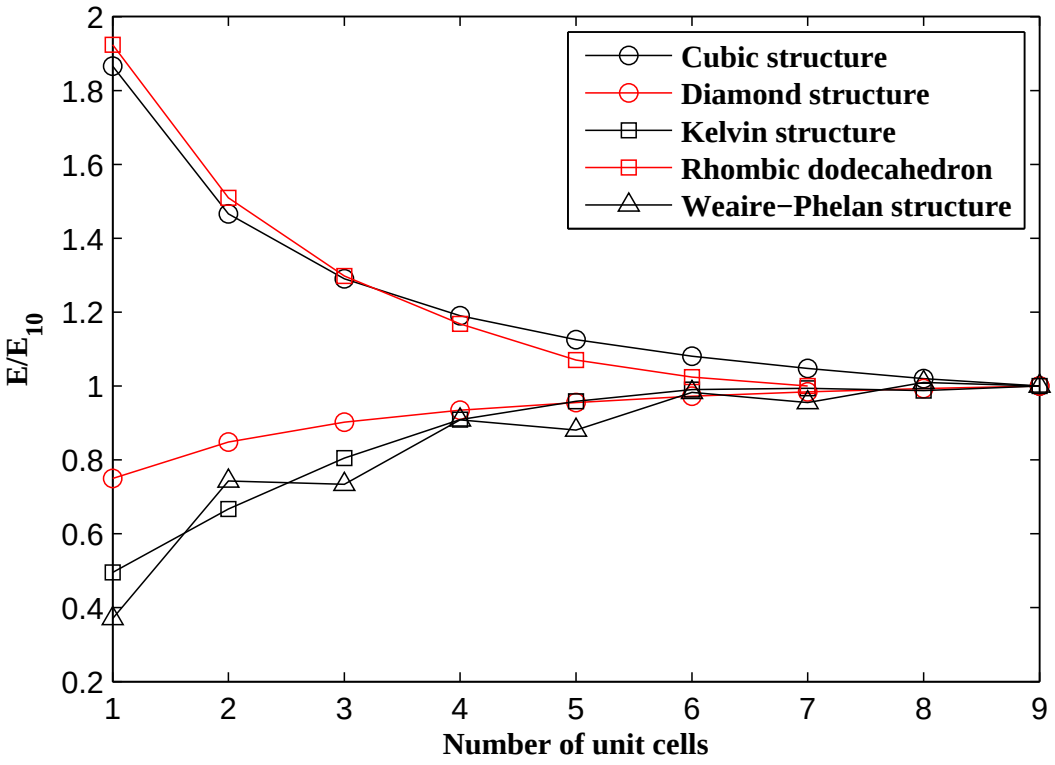

Figure 3- Ratio of Young's modulus E of lattice structures with different unit cell numbers to the Young's modulus of the corresponding lattice structures with 10 unit cells E_{10}

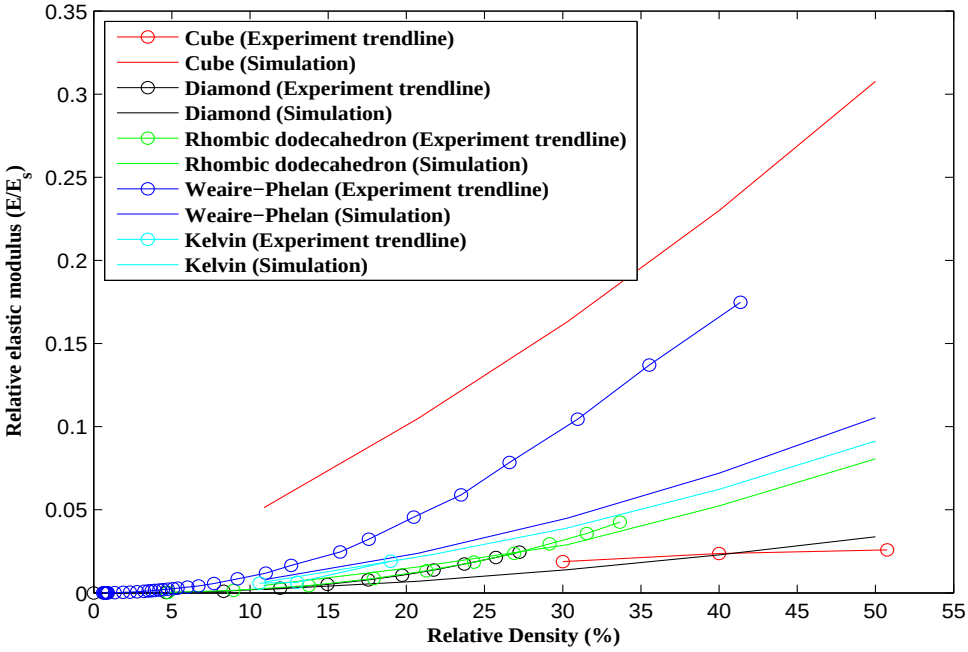

(a)

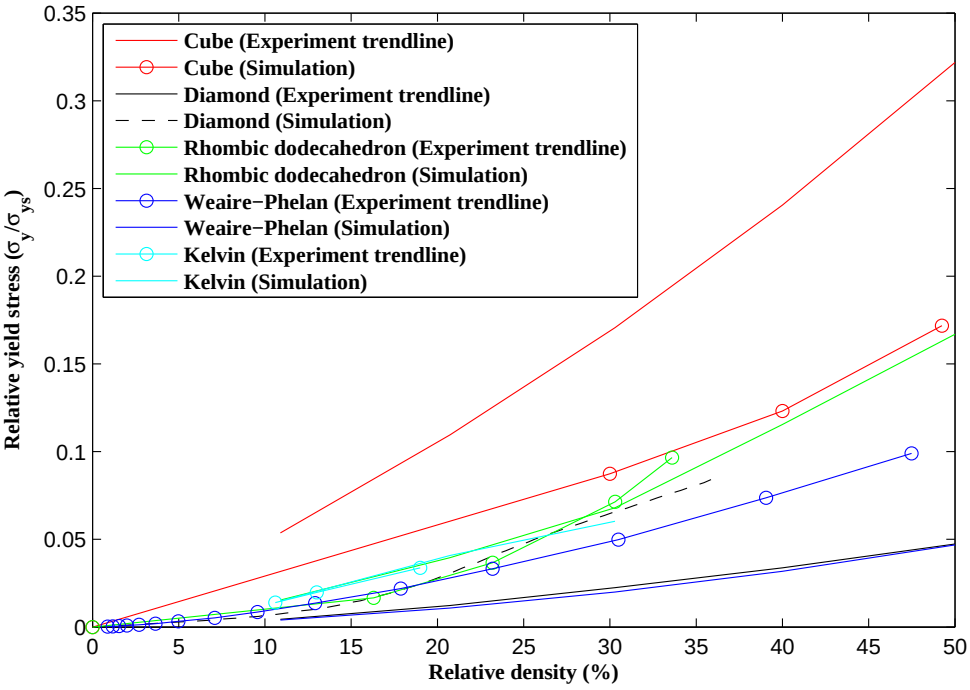

(b)

Figure 4- Comparison of numerical and experimental (a) elastic modulus and (b) yield stress for the unit cell types considered in this study

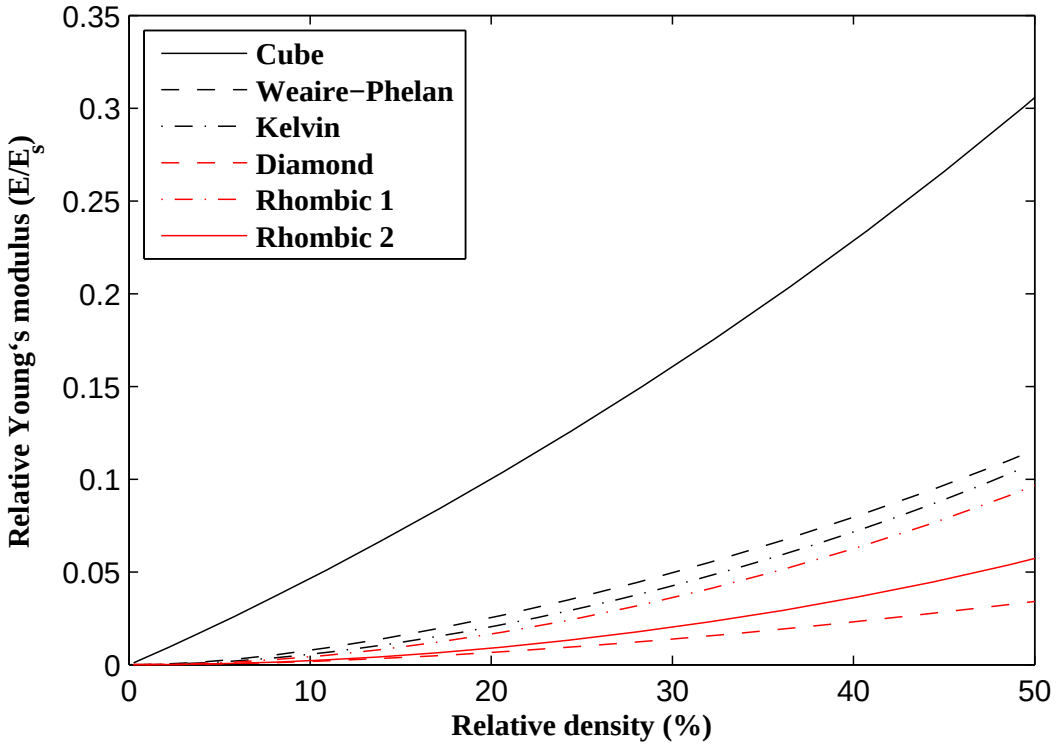

Figure 5- Effect of unit cell type on the porous structure Young's modulus

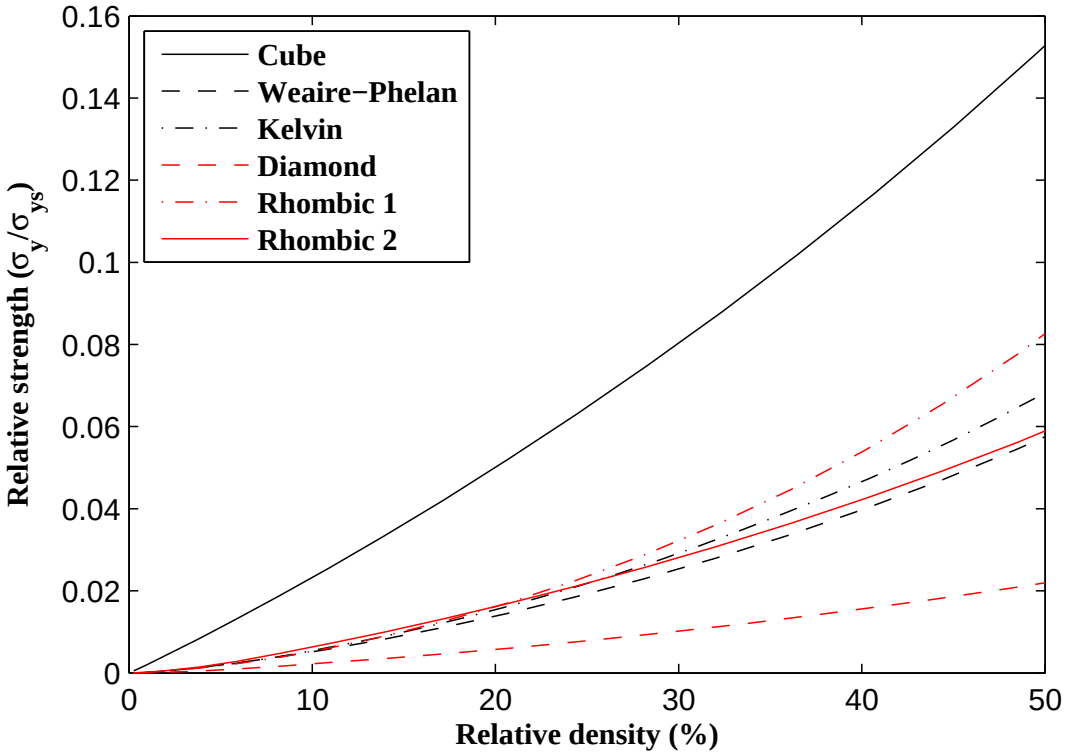

Figure 6- Effect of unit cell type on the porous structure yield stress

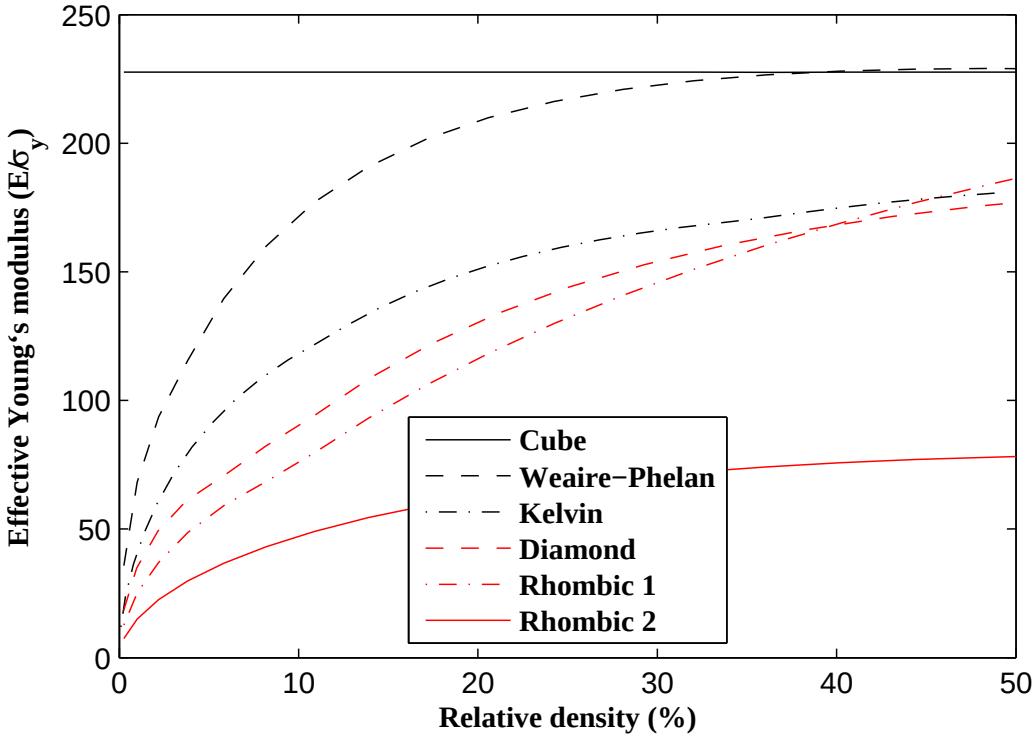

Figure 7- Effect of unit cell type on the porous structure effective Young's modulus ($\frac{E}{\sigma_y}$)

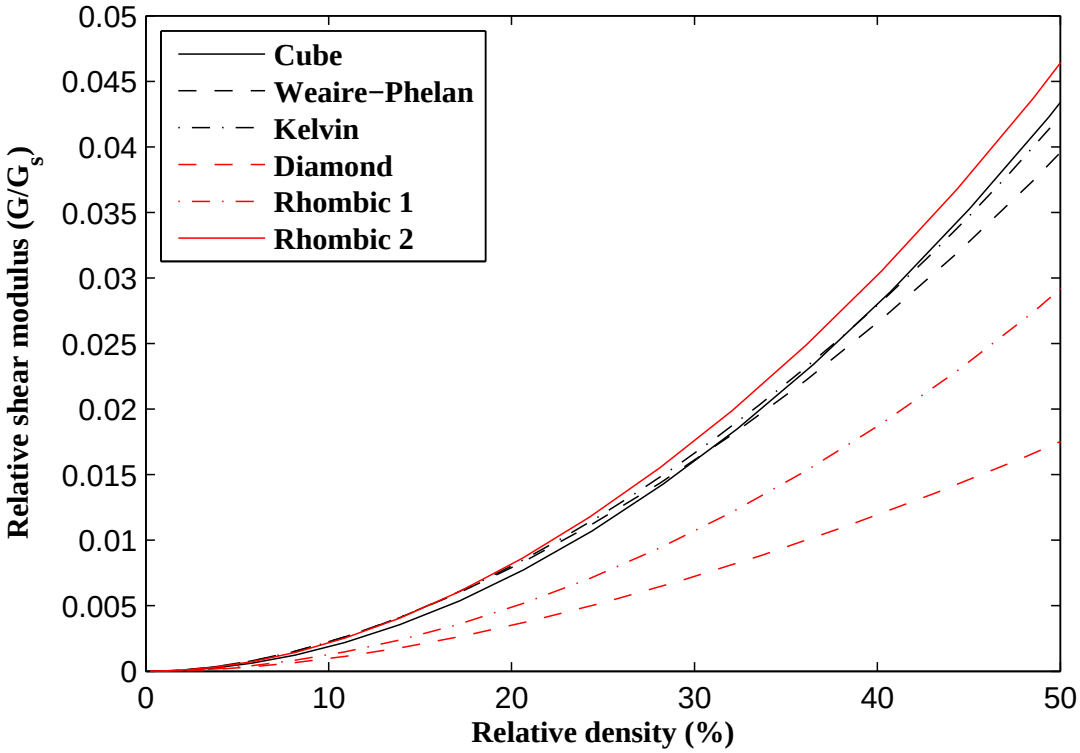

Figure 8- Effect of unit cell type on the porous structure shear modulus

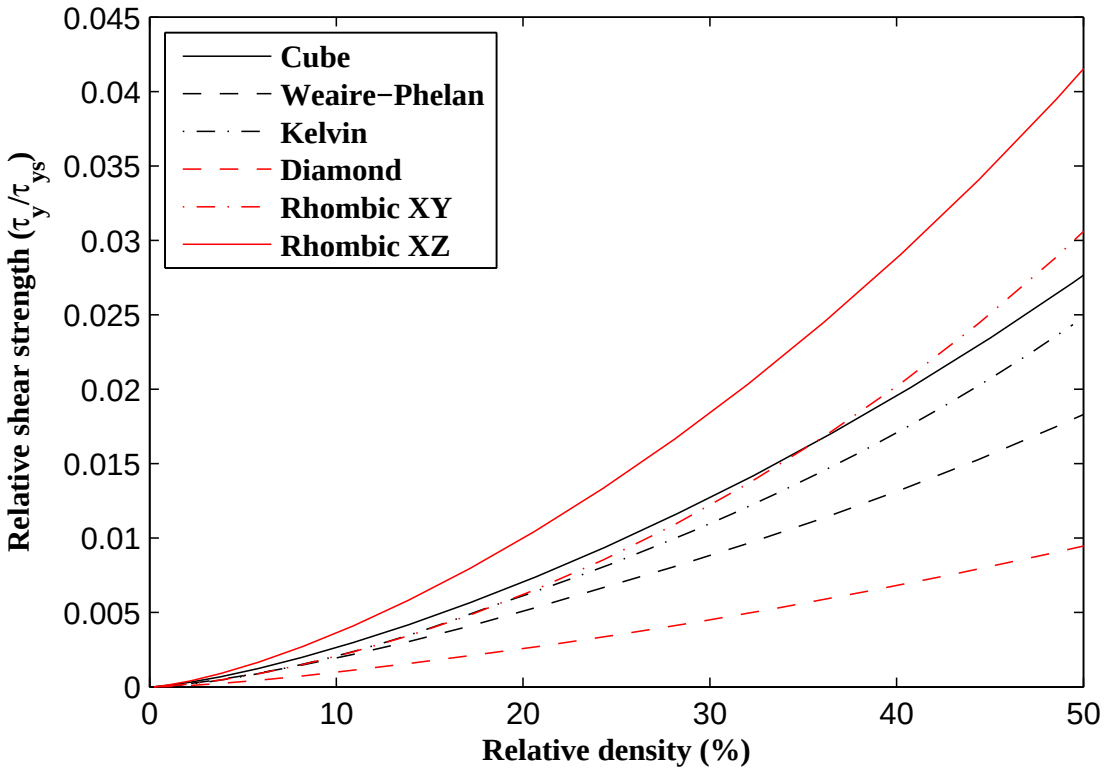

Figure 9- Effect of unit cell type on the porous structure shear yield stress

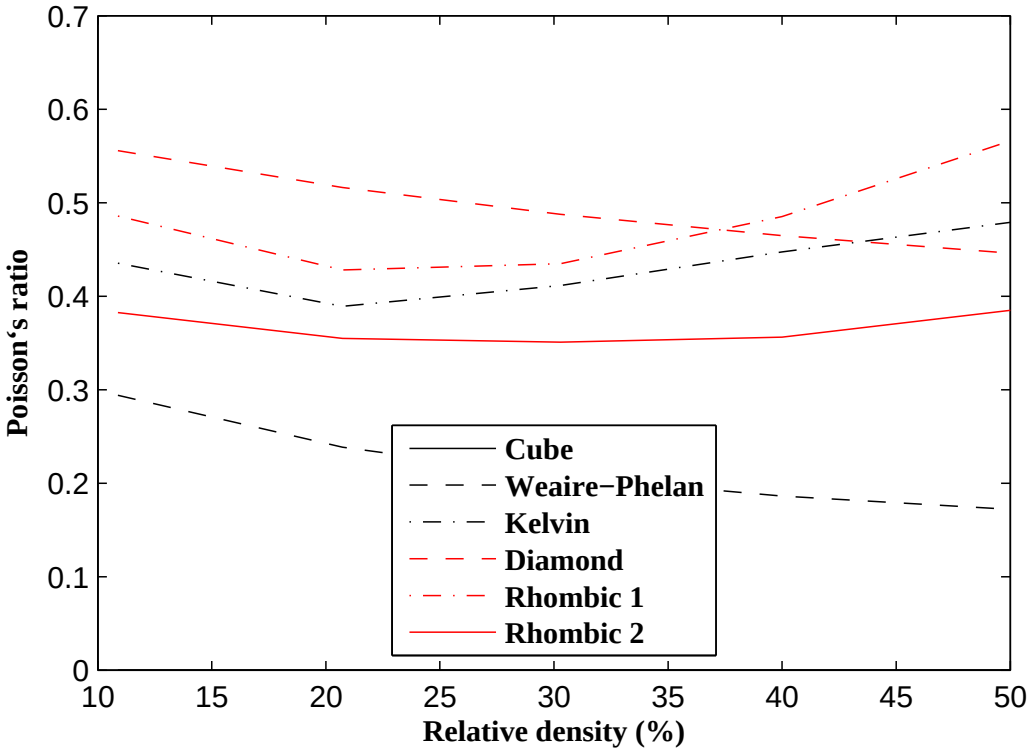

Figure 10- Effect of unit cell type on the porous structure Poisson's ratio

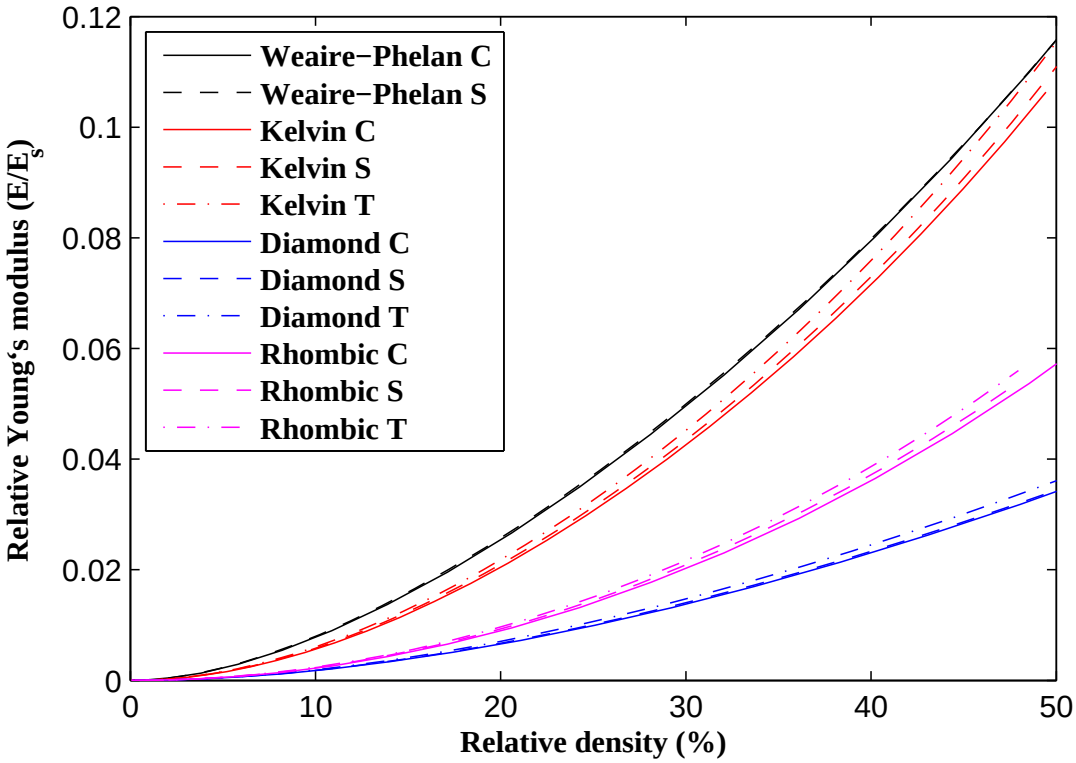

Figure 11- Effect of cross-section type on the structure Young's modulus (C, S, and T stand for Circular, Square, and Triangular cross-sections, respectively)

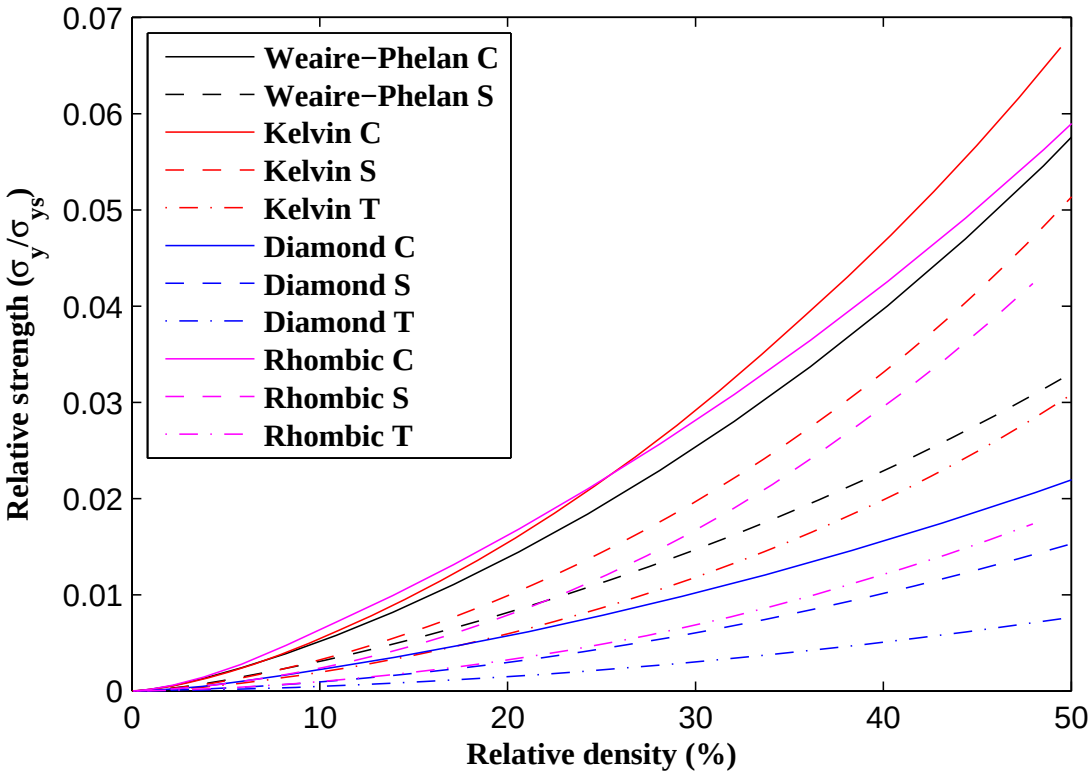

Figure 12- Effect of cross-section type on structure yield stress (C, S, and T stand for Circular, Square, and Triangular cross-sections, respectively)

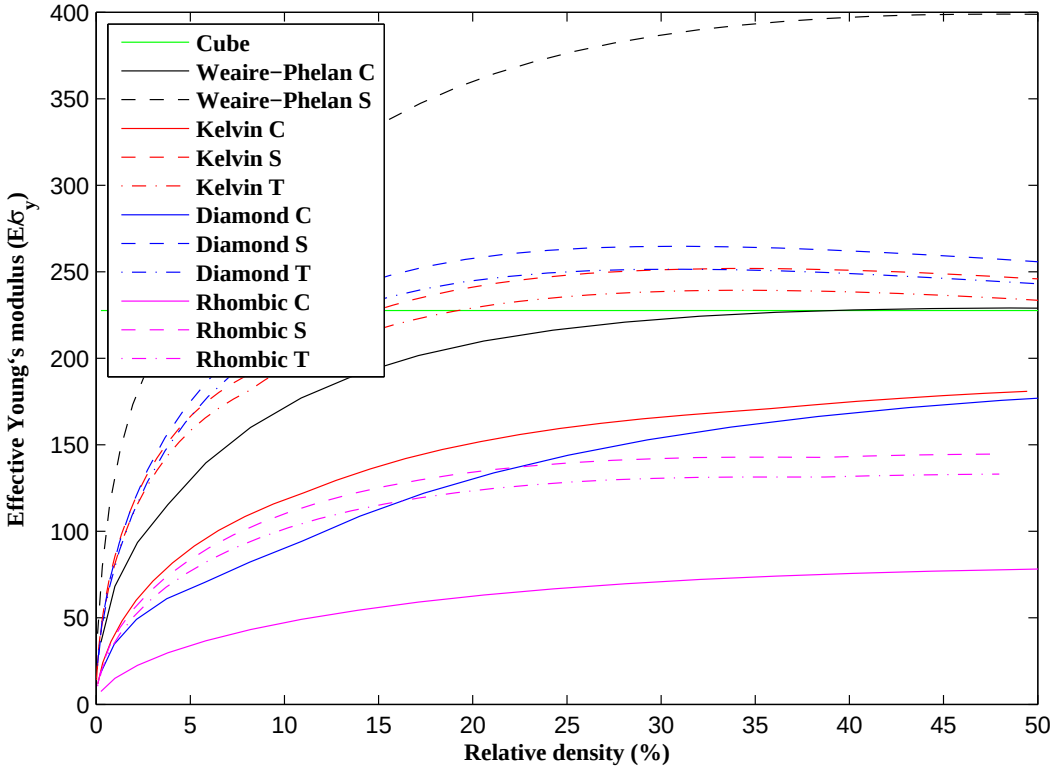

Figure 13- Effect of cross-section type on the structure effective Young's modulus ($\frac{E}{\sigma_y}$) (C, S, and T stand for Circular, Square, and Triangular cross-sections, respectively)

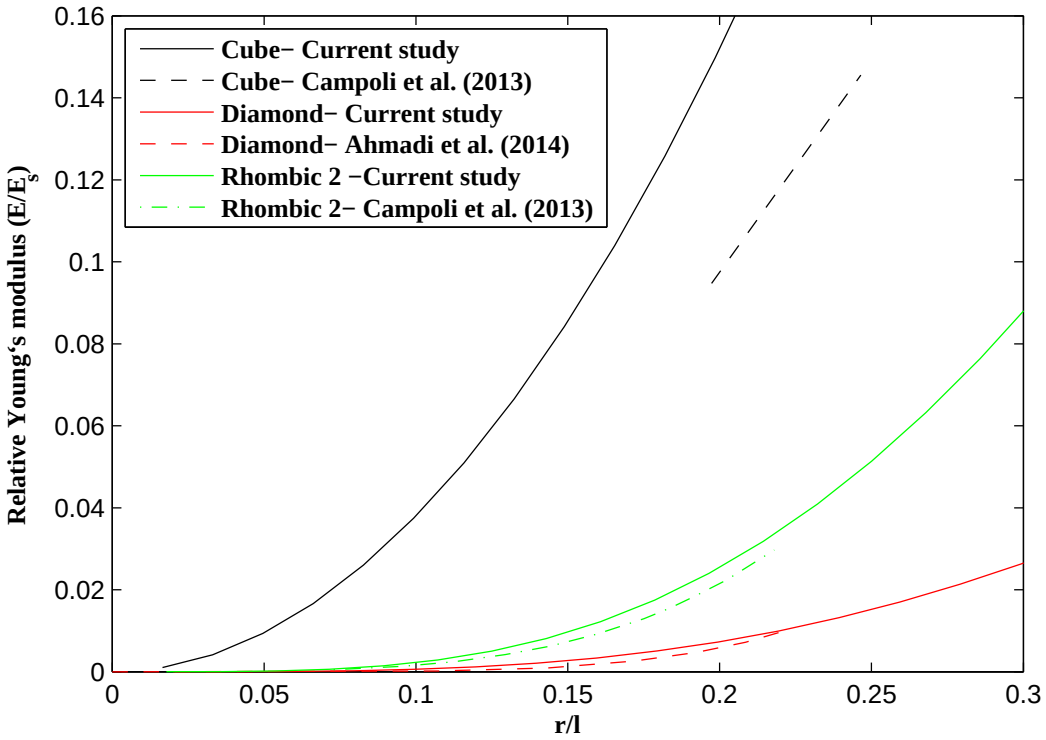

Figure 14- Comparison of the numerical results of this study to the corresponding numerical results in [12, 16]